Investigating zonal asymmetries in stratospheric ozone trends from satellite limb observations and a chemical transport model

C. Arosio[1], M. P. Chipperfield[2,3], S. Dhomse[2,3], W. Feng[2], A. Rozanov[1], M. Weber[1], X. Zhou[2,4] and J. P. Burrows[1]

[1]Institute of Environmental Physics, University of Bremen, Bremen, Germany
[2]School of Earth and Environment, University of Leeds, Leeds, UK
[3]National Centre for Earth Observation (NCEO), University of Leeds, Leeds, UK
[4]School of Atmospheric Sciences, Chengdu University of Information Technology, Chengdu, China

Key Points:

- A longitudinal asymmetry in stratospheric ozone trends at northern high latitudes is found in satellite observations in the past two decades
- The asymmetry is particularly large in springtime and the TOMCAT chemistry transport model well reproduces the pattern
- Changes in polar wave activity and in the position and strength of the polar vortex are found to be relevant to explain this pattern

Corresponding author: Carlo Arosio, `carloarosio@iup.physik.uni-bremen.de`

Abstract

This study investigates the origin of the zonal asymmetry in stratospheric ozone trends at northern high latitudes, identified in satellite limb observations over the past two decades. We use a merged dataset consisting of ozone profiles retrieved at the University of Bremen from SCIAMACHY and OMPS-LP measurements to derive ozone trends. We also use TOMCAT chemical transport model (CTM) simulations, forced by ERA5 reanalyses, to investigate the factors which determine the asymmetry observed in the long-term changes. By studying seasonally and longitudinally resolved observation-based ozone trends, we find, especially during spring, a well-pronounced asymmetry at polar latitudes, with values up to +6 % per decade over Greenland and -5 % per decade over western Russia. The control CTM simulation agrees well with these observed trends, whereas sensitivity simulations indicate that chemical mechanisms, involved in the production and removal of ozone, or their changes, are unlikely to explain the observed behaviour. The decomposition of TOMCAT ozone time series and of ERA5 geopotential height into the first two wavenumber components shows a clear correlation between the two variables in the middle stratosphere and demonstrates a weakening and a shift in the wavenumber-1 planetary wave activity over the past two decades. Finally, the analysis of the polar vortex position and strength points to a decadal oscillation with a reversal pattern at the beginning of the century, also found in the ozone trend asymmetry. This further stresses the link between changes in the polar vortex position and the identified ozone trend pattern.

Plain Language Summary

Monitoring long-term ozone changes in the stratosphere is important to assess the evolution of the ozone layer in response to the Montreal Protocol and climate changes. In this study, we investigate the origin of a zonal asymmetry in stratospheric ozone trends over the past two decades, which was identified at northern polar latitudes by analyzing satellite observations. To this aim, we use a merged dataset consisting of ozone profiles retrieved at the University of Bremen from SCIAMACHY and OMPS-LP measurements to derive ozone trends. We also use TOMCAT chemical transport model (CTM) simulations to investigate the factors which determine the asymmetry observed in the long-term ozone changes. The asymmetry is found to be largest in springtime, and the CTM simulation agrees well with the observation-based trends. Sensitivity simulations indicate that chemical mechanisms, involved in the production and removal of ozone, are unlikely to explain the observed pattern. On the contrary, changes in atmospheric dynamics are found to be relevant. In particular, the analysis of the polar vortex position and strength points to a decadal oscillation with a reversal pattern at the beginning of the century, which is also found in the ozone trend asymmetry.

1 Introduction

The variations of the ozone concentration, as a function of time, altitude and latitude are explained by several dynamical, chemical and photochemical processes (e.g., Seinfeld & Pandis, 2016; WMO, 2022). In the lower stratosphere, where the chemical lifetime is relativity long (i.e. many years), except during polar spring, ozone is transported from the tropics to high latitudes, and it is affected by changes in atmospheric dynamics. In the upper stratosphere ozone has a relatively short photochemical lifetime, implying that changes in the transport of long-lived chemical species and in temperature play important roles in determining ozone concentrations at those levels.

The stratospheric circulation comprises an upper branch of the Brewer–Dobson circulation (BDC), involving upwelling in the tropics, meridional poleward transport, and then descent in the polar regions, and a lower branch, having a more rapid meridional poleward transport on isentropic surfaces (Butchart, 2014). This circulation is driven

by the wave breaking in the stratosphere and therefore is subject to strong inter-annual variability. The wave breaking happens in the so called "surf zone" at the edge of the polar vortex, so that its position and vertical structure has an indirect impact on the BDC, as well as BDC impacts the vortex position and strength (McIntyre & Palmer, 1984). An acceleration of the stratospheric mean mass transport has been predicted by several model studies (e.g., Garcia & Randel, 2008), but strong inter-annual variations prevent a robust detection of this trend from observations. In addition there may be decadal–scale oscillations. A large inter-annual variability also characterizes the polar vortex, with climate models not agreeing on whether it will weaken or strengthen during the 21st century (Karpechko et al., 2022). Several studies have addressed decadal changes of the polar vortex position and strength (e.g., Zhang et al., 2016; Seviour, 2017), pointing out a vortex weakening and shift of its mean position towards Eurasia, particularly at the end of the last century. In contrast, Hu et al. (2018) presented a strengthening of the stratospheric polar vortex over the last two decades, that could be related to a weakening of the propagation of wavenumber-one wave flux, which was connected by the authors to sea-surface temperature warming over the north Pacific sector.

Among various anthropogenic influences on the stratospheric ozone, two most relevant are the release of halogen-containing ozone-depleting substances (ODSs) and of greenhouse gases (GHGs). With the adoption of the Montreal Protocol and its amendments the industrial production of ODSs, e,g. chlorofluorocarbon compounds (CFCs), was regulated. This reduced their emissions during the 1990s and is expected to lead to a recovery of the ozone layer globally (e.g., WMO, 2018, 2022). On the other hand, the increasing concentration of GHGs such as CO_2 and CH_4 in the troposphere, is causing a cooling of the stratosphere, through radiative transfer feedback. This cooling affects the ozone chemistry in the upper stratosphere, as the rate coefficients of reactions involved in catalytic cycles removing ozone have a direct dependence on temperature (Waugh et al., 2009). At the same time, the termolecular reaction $O_2 + O + M \rightarrow O_3 + M$ has a rate inversely proportional to temperature so that the cooling also accelerates the ozone production (Groves et al., 1978).

The coupling between the described chemical and dynamical processes controlling stratospheric ozone is expected to have a complex spatial structure, varying in altitude, latitude, longitude and time. Therefore, to study long-term variations of the ozone field, there is a need for consistent long-term time series with a good temporal and spatial coverage over the whole globe.

In order to study long-term changes in ozone vertical profiles and test our understanding of the impact of natural phenomena and anthropogenic activities on atmospheric ozone, single instrument time series are generally inadequate. Several studies have used satellite merged datasets to investigate stratospheric ozone trends, but the majority of them focused only on zonal mean changes (e.g., WMO, 2022). By exploiting the dense spatial sampling provided by limb observations, recently, Arosio et al. (2019) and Sofieva et al. (2021) looked at longitudinally resolved trends and highlighted the presence of zonal asymmetries, especially at northern high latitudes. In particular, poleward of 60 °N, they identified a bi-polar structure having positive values over the Atlantic/Greenland sector and close to zero or negative changes over Siberia.

As discussed in the following paragraphs, some studies also showed zonal asymmetries in the BDC and its impact on the distribution of trace gases and ozone trends in winter-time at northern high latitudes, by using model simulations and satellite datasets. Most studies focused on total ozone column measurements.

Longitudinally varying changes in total ozone were already pointed out in the study by Hood and Zaff (1995), who investigated total ozone at northern mid-latitudes during winter in the 1980s, using TOMS measurements. The authors identified the typical asymmetric ozone distribution related to quasi-stationary planetary waves, i.e. a pro-

nounced maximum over eastern Russia related to the Aleutian low and a secondary maximum over eastern Canada associated with the Icelandic low. In addition, a distinct longitudinal dependence of the mid-latitude ozone trends over this period was identified: the largest negative trends (-40 DU per decade) occurred over Russia and western Pacific, whereas positive trends were found over the northern Atlantic sector. Another study using TOMS data was performed by Peters and Entzian (1999) who investigated decadal total ozone changes in the months December-February over the period 1979-1992 in the northern hemisphere. They found a strong anti-correlation between the long-term total ozone changes and the 300-hPa geopotential height (GPH) changes. This means that decadal changes in the UTLS dynamics led to longitude-dependent changes in the total ozone.

Asymmetries in the ozone climatology were investigated by Bari et al. (2013), using models, reanalysis and satellite data, focusing on the northern mid-latitudes in winter. The authors stressed the importance of a 3-D approach in studying the BDC. They found that the distribution of winds and trace gases is related to the zonal wavenumber-1 pattern in geopotential hight (GPH) observed in the northern hemispheric stratosphere during winter at high and mid-latitudes. They showed that air masses are driven southwards and upwards to the upper stratosphere over the Pacific ocean, whereas over Europe and Asia the flow is northward and downward.

More recently, Kozubek et al. (2015) investigated the meridional component of stratospheric winds as a function of altitude at northern mid-latitudes to study its longitudinal dependency. A well-defined two-core structure was identified at 10 hPa in the northern hemisphere, with opposite wind directions, related to the Aleutian pressure high at 10 hPa. They also computed meridional wind changes over two periods: 1970-1995 and 1996-2012. They found that meridional wind trends are negative in the first period and positive in the second period, i.e. the two-core structure became stronger in the last 2 decades. As a follow up, Kozubek et al. (2017) investigated the long-term variations of stratospheric winds over the whole globe at 10 hPa using four reanalysis datasets. The trends were reported for winter months before and after the ozone trend turnaround point at the end of the 1990s. They found hints of an acceleration of the BDC and change in the ozone trend asymmetries before and after 1997.

Within this framework, and in light of the findings in Arosio et al. (2019) and Sofieva et al. (2021), the present paper aims to analyze vertically and longitudinally resolved ozone trends from satellite observations and to exploit simulations from the TOMCAT chemistry transport model (CTM) to identify the mechanisms driving the observed zonal asymmetry in the ozone linear trends in the period 2004 to 2021. Sect. 2 introduces the satellite dataset used in this study and the TOMCAT CTM. Sect. 3 shows a comparison of the measured and simulated ozone anomalies and of the respective zonally and longitudinally resolved trends, where the asymmetry at northern high latitudes is evident. Sect. 4 presents the results of TOMCAT runs, which were designed to assess the impact of chemical processes on the observed longitudinally asymmetric pattern in ozone trends. In Sect. 5 we explore in more detail the seasonally-resolved long-term changes in ozone and temperature, which leads to Sect. 6 where geopotential height and ozone fields are decomposed into wavenumber-1 and -2 to assess similarities in their behaviour. Finally, in Sect. 7 we present some potential vorticity trends to further investigate changes in the polar vortex over the past two decades, followed by concluding remarks.

2 Datasets

2.1 Satellite observations

The merged satellite dataset consisting of observations from the SCanning Imaging Absorption spectroMeter for Atmospheric CHartographY (SCIAMACHY) and the

Ozone Mapper and Profiler Suite - Limb Profiler (OMPS-LP) has been produced at the University of Bremen and is described in Arosio et al. (2019). Here, it will be referred to as SCIA+OMPS. This dataset is longitudinally resolved with a grid size of 5° in latitude and 20° in longitude and has a vertical resolution of 3.3 km. The time series has been recently updated after the re-processing of the OMPS-LP dataset by using improved Level 1 gridded (L1G) data. In the new L1G data version (v2.6), the NASA team implemented some calibration corrections, a wavelength registration adjustment and an improved pointing correction. The main aim of the re-processing is the removal of the positive drift identified in the previous OMPS-LP ozone product with respect to independent time series (Kramarova et al., 2018), e.g., from the Microwave Limb Sounder (MLS), which has proven its long-term stability in previous studies, e.g., Hubert et al. (2016). We define the drift as the linear trend of the relative difference between OMPS-LP and MLS.

The drift w.r.t. MLS time series is shown in Fig. 1. The left panel refers to the OMPS-LP time series retrieved using L1G v2.5 data, whereas the right panel refers to the updated time series, based on L1G v2.6 data. The comparison between the left and the right panel shows that the strong positive drift w.r.t. MLS has been significantly reduced, particularly above 35 km. The striped areas indicate values which are lower than the respective 2σ uncertainty, i.e. they are not statistically significant at 95 % confidence level. Drift values are still significant at some altitude-latitudes but generally with values half as large as for the previous data version. This result provides improved confidence in the scientific value of the ozone trends derived from the SCIA+OMPS merged time series.
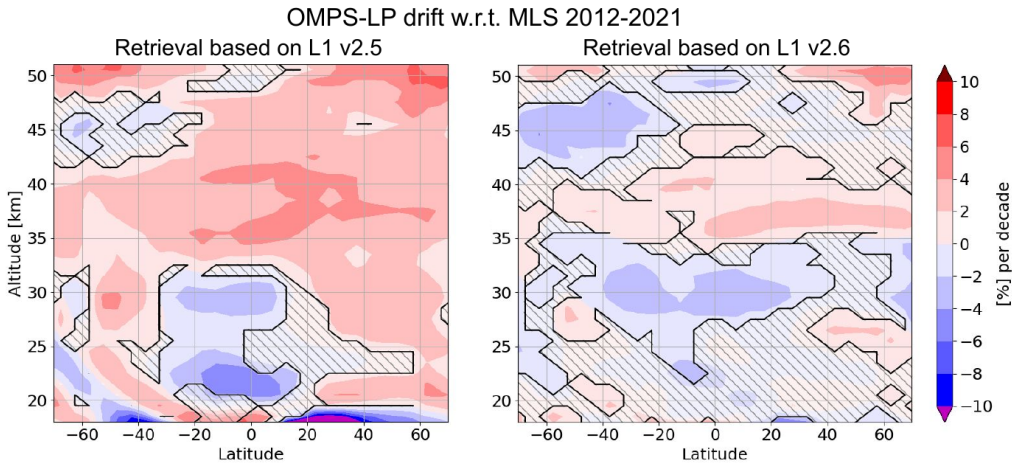

Figure 1. Drift of the OMPS-LP ozone product retrieved at the University of Bremen w.r.t. MLS during the period 2012-2021 in % per decade. Left panel: using L1G v2.5 data. Right panel: using L1G v2.6 data. Striped areas are non-significant at 2σ.

2.2 TOMCAT chemical transport model

TOMCAT/SLIMCAT is a three-dimensional off-line chemical transport model (CTM) (M. Chipperfield, 2006). The model is forced by winds and temperatures from meteorological analyses, which, in this study, are taken from the European Centre for Medium-Range Weather Forecasts (ECMWF) reanalysis v5 (ERA5). Once the atmospheric transport and temperatures are prescribed, the model calculates the abundances of chemical species in the troposphere and stratosphere. A full-chemistry reference run was used as baseline for this study and other dedicated runs were produced. The resolution of the model was kept 2.8° × 2.8° latitude and longitude, and about 1.5 km altitude in the strato-

sphere, and was interpolated to match the merged satellite dataset resolution. Monthly averaged values are considered.

The TOMCAT CTM simulations were used in this study for three important reasons:

1. The CTM provides a continuous time series without spatial or temporal gaps, so that it is possible, for example, to explore polar winter conditions, which are not sampled by limb scattering sounders;
2. The possibility to study trends going back in time until 1979, when satellite limb observations were sparse;
3. The possibility to investigate the mechanisms that determine the trend asymmetries by running dedicated simulations using different settings.

3 Comparison with TOMCAT: time series and trends

As a preliminary consistency check, we looked into the absolute bias between SCIA+OMPS and TOMCAT time series, and noticed that the CTM underestimates ozone content in the upper stratosphere and overestimates it in the lower stratosphere, which is a known feature (Dhomse et al., 2021): further investigations on this issue are outside the scope of this paper. For this reason and because we are interested in ozone trends, deseasonalized (relative) anomalies of the time series were calculated and found to be in good agreement with SCIA+OMPS, as shown in Fig. 2. In the lower tropical stratosphere, the amplitude of the oscillations, probably due to the Quasi Biennial Oscillation (QBO), is more pronounced in TOMCAT than in SCIA+OMPS. MLS time series is also included as a reference in this plot.
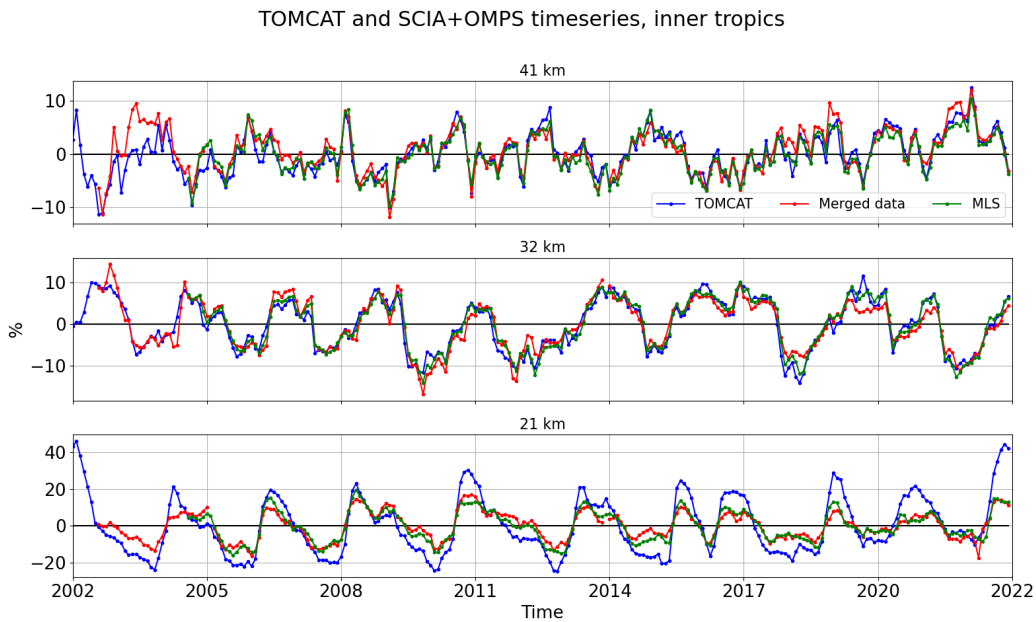

Figure 2. Deseasonalized anomalies from the reference TOMCAT simulation, the merged SCIA+OMPS dataset and MLS time series, in the inner tropics ([5° S, 5° N]) at three altitudes (41, 32 and 21 km).

We applied to both TOMCAT and SCIA+OMPS time series a multivariate linear regression model, based on the Long-term Ozone Trends and Uncertainties in the Stratosphere (LOTUS) model and including several proxies. In particular, we included in the regression model traditionally employed proxies (e.g., Petropavlovskikh et al., 2019), such as the first two principal components of the QBO, the Multivariate El Nino Southern Oscillation (ENSO) index (MEI) and the Mg II index for solar activity, but also dynamical proxies such as the yearly integrated eddy heat fluxes and the Atlantic/Antarctic oscillation (AO/AAO). For a more detailed description of the used proxies, we refer to Weber et al. (2022).

Due to the discrepancies in the SCIAMACHY time series w.r.t. other satellite products found in the first year of its lifetime (Sofieva et al., 2017), and because of the Hunga Tonga volcanic eruption, which occurred in January 2022, with its large stratospheric perturbation (Lu et al., 2023), we focused on the period 2004-2021 to study ozone trends.

The resulting zonal mean ozone trends are reported in Fig.3. Striped areas also in the following plots indicate values which are smaller than the 2σ uncertainty (non-significant).
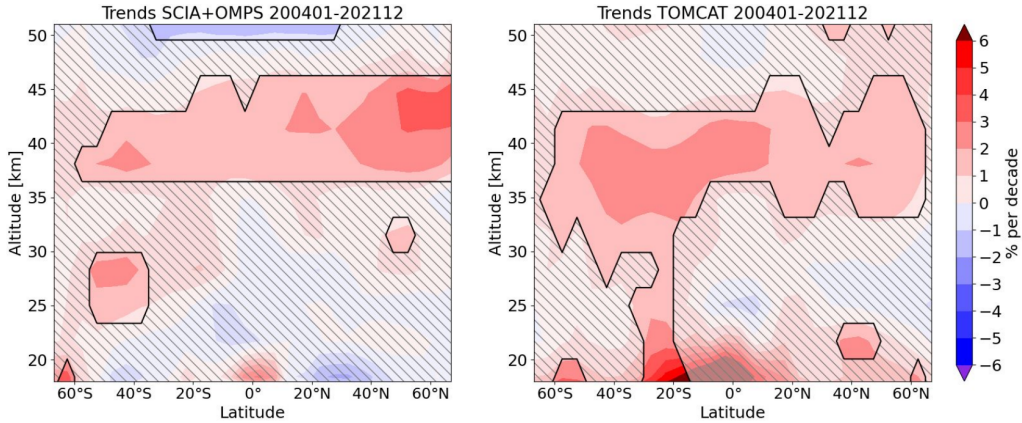

Figure 3. Zonal mean ozone trends from SCIA+OMPS on the left and from TOMCAT on the right, computed over the 2004-2021 period. Striped areas are non-significant at 2σ.

Generally a good agreement between model and observations is found, with the expected positive trends in the middle and upper stratosphere, related to the ongoing ozone recovery. The most significant discrepancy is located below 25 km where TOMCAT shows overall positive trends, whereas SCIA+OMPS shows negative values, though non-significant, except for the inner tropics at 19 km. The detection of negative trends in the lower tropical and extra-tropical stratosphere has been extensively debated (Ball et al., 2018; M. P. Chipperfield et al., 2018). A possible reason for the discrepancy between TOMCAT and SCIA+OMPS in the lower stratosphere is related to ERA5 forcing, as pointed out by Li et al. (2022, 2023).

In comparison with the long-term 2000-2020 ozone trends shown in Godin-Beekmann et al. (2022), trend values in the lower stratosphere are not significant and closer to zero. The negative values identified in SCIA+OMPS above 47 km are not shown by other merged datasets.

Longitudinally resolved trends from TOMCAT and SCIA+OMPS are compared in Fig. 4, at a specific altitude (38 km), in terms of stratospheric ozone column (SOC) and for a longitude-altitude cross section at 67.5° N. In the top row, we notice a pronounced longitudinal variability and some common patterns in CTM and in SCIA+OMPS

trends, especially the zonal asymmetry above 45° N. This asymmetry is more evident
in TOMCAT, with negative (though non-significant) values over the Siberian and East-
Canadian sectors, and positive values over the Atlantic sector. Looking at the plot show-
ing the trends in SOC and the longitude-altitude cross section at 67.5° N, we can see that
the asymmetry is vertically consistent. The positive SOC trend in the Atlantic sector
are significant at 2σ, especially for TOMCAT. A similar structure was identified also in
MLS time series and in the MEGRIDOP dataset (Sofieva et al., 2021). Above 35 km,
TOMCAT shows smaller positive values over the Atlantic sector as compared to the satel-
lite observations. To further test the robustness of this pattern and its independence from
ERA5 forcing, in the Supplements, in Fig. S2 we compared trends from the MERRA 2
- Global Modeling Initiative (M2-GMI) CTM time series, which is forced with MERRA-
2 meteorology, with TOMCAT, and found a bias in term of absolute trend values but
a good agreement in terms of asymmetric pattern.
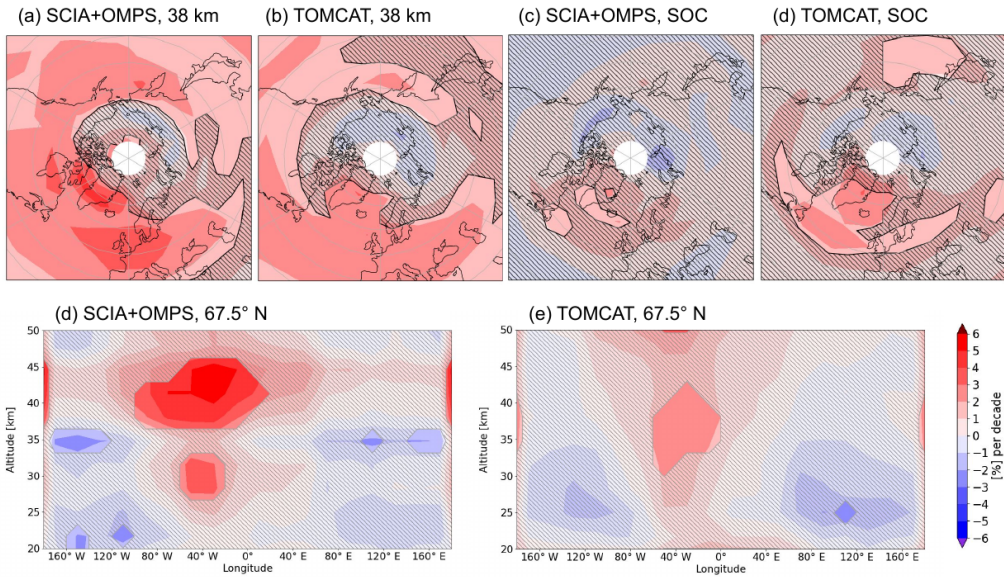
Figure 4. Top row: longitudinally resolved trends for SCIA+OMPS (panel a) and TOMCAT
(panel b) datasets at 38 km, in terms of stratospheric columns for both datasets in panels (c) and
(d) resepctively. Bottom row: trends for a longitude-altitude cross section at 67.5° N. Striped
areas denote non-significant values at 2σ level.

A TOMCAT simulation with a higher spatial resolution (1.4° × 1.4° × 0.75 km
grid) was run to investigate whether the discrepancies between the CTM and SCIA+OMPS
could be reduced. This simulation was sampled at the locations of the satellite obser-
vations to make the CTM time series more consistent with the merged dataset, in terms
of temporal and spatial sampling. The resulting dataset was re-gridded and the two parts
of the time series, covering SCIAMACHY and OMPS-LP periods respectively, were de-
biased to remove the discrepancy related to the different local time of the satellite ob-
servations. The comparison of the resulting higher resolution data did not show any sig-
nificant differences w.r.t. the standard run, neither in the trends nor in the time series
(here not shown). As a result, we use the standard run as reference in this study.

4 Investigation of the potential influence of chemical processes on the trend asymmetry

We performed two additional sensitivity (SEN) simulations to investigate the potential influence of chemical processes on the origin of the ozone trend asymmetry. The first simulation 'SEN-fDyn' was forced using constant ERA5 data, corresponding to the year from July 1999 to June 2000, which were repeated each year over the 2004-2021 period. The choice of the 1999/2000 year is arbitrary, as far as a winter with an average-strong polar vortex is considered; we tested the use of the July 2002 to June 2003 period for the repeating forcing without finding any significant difference. In the second simulation 'SEN-noPSC', polar stratospheric clouds (PSCs)-related heterogeneous chemistry was inhibited, by not allowing temperature to drop below 200 K in the model chemistry scheme to prevent PSC formation. The results are shown in Fig. 5. The longitude-altitude cross section of the ozone trends at 67.5° N over 2004-2021 from the reference full-chemistry TOMCAT (control) run is shown, together with the trends for the 'SEN-noPSC' and 'SEN-fDyn' simulation.

Fig. 5 shows that the zonally asymmetrical trend pattern from the SEN-noPSC simulation is almost identical to the one from the control simulation. As expected, the trends over the Atlantic sector are smaller due to reduced ozone losses in the absence of PSCs. This indicates that heterogeneous chemistry does not play a relevant role in producing trends variable with longitude. To further test this hypothesis and the robustness of the zonal asymmetry we computed the ozone trends for the 2004-2019 period, i.e. excluding the cold 2019/2020 Arctic winter. As discussed in the Supplements, Fig. S1, we did not find relevant differences, highlighting the robustness of the pattern.

Trend values in the 'repeating forcing' scenario show zonal symmetry and are overall smaller with respect to the reference run. In this case no long-term temperature trend is present in the forcing, which plays an important role for the ozone trend in the upper stratosphere. The fact that no zonal asymmetry is observed for this run indicates that gas-phase chemistry alone cannot directly explain either the asymmetry in trends. However, an indirect impact of atmospheric dynamics on gas-phase chemistry cannot be excluded (Galytska et al., 2019).

In addition, we compared the trend results computed for the TOMCAT reference run and for ERA5 ozone data. As shown in Fig. 6, the zonal trends in ERA5 are significantly different from Fig. 3, pointing out that ozone reanalysis data should not be used to compute long-term ozone changes, unless a careful de-biasing of the time series is performed (e.g., Bernet et al., 2020). However, longitudinally resolved trends shown in Fig. 6 at 32 km have a remarkable similarity with the pattern found in TOMCAT. This provides more evidence that atmospheric dynamics is mainly driving the observed asymmetric pattern, as TOMCAT is forced with ERA5 meteorology.

5 Seasonal ozone trends

To further investigate the longitudinal asymmetry at northern high latitudes, seasonal trends were analyzed. Two approaches to obtain seasonal time series for the SCIA+OMPS dataset are described in Appendix Appendix A. In the following, we show trend values obtained by merging the two seasonally averaged single-instrument time series.

In Fig. 7, seasonal ozone trends are shown for SCIA+OMPS (top row) and for the reference TOMCAT run (middle row) at 32 km altitude for spring (MA), summer (JJA) and autumn (SO). Only two months are used in spring and autumn to get a better coverage of the polar regions. The TOMCAT time series was masked to mirror the availability of satellite data. ERA5 temperature trends are displayed in the bottom row of Fig. 7 for the same three seasons.
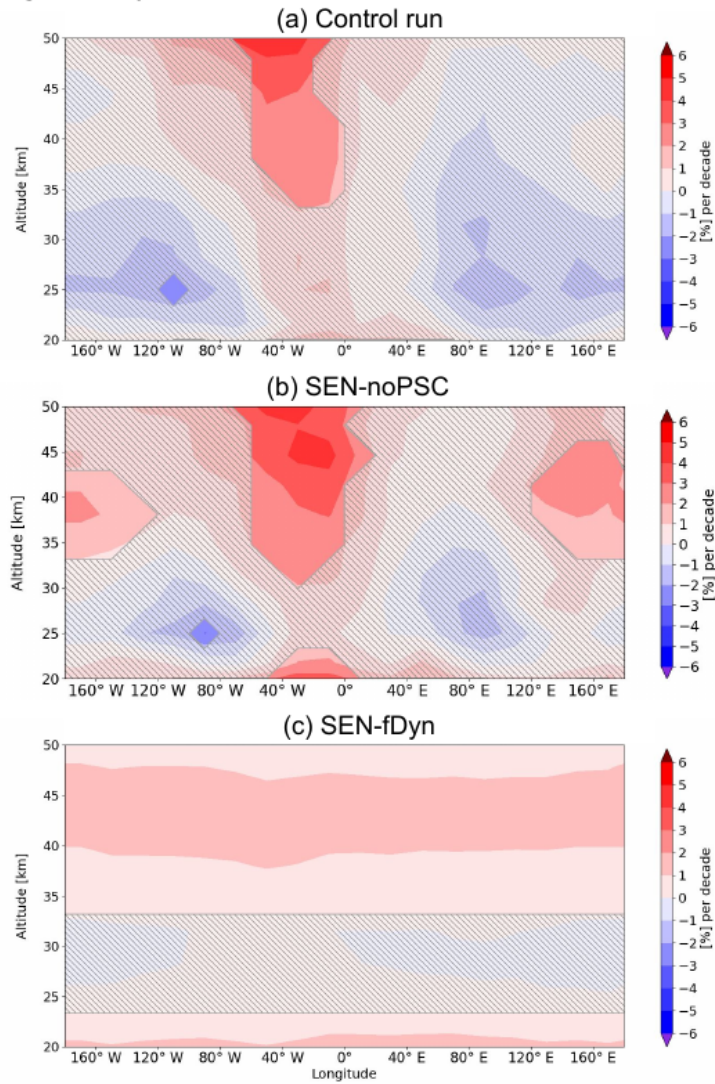
Figure 5. Longitudinally-resolved ozone trend cross section at 70° N, over 2004-2021 for three TOMCAT scenarios: (a) reference control run, (b) PSC-inhibited scenario and (c) repeating forcing.
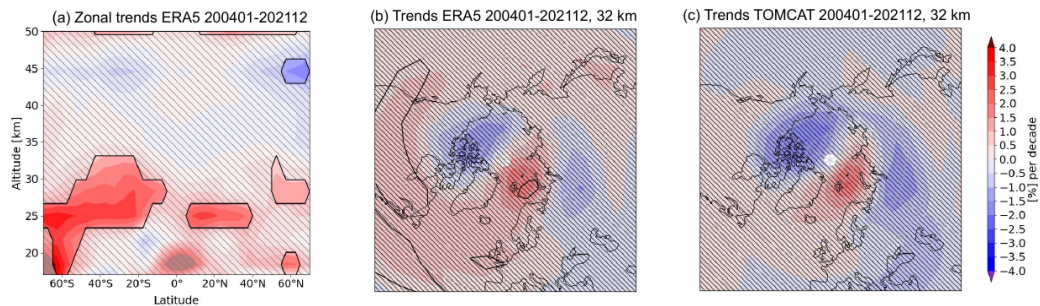

Figure 6. Panel (a) shows zonal ozone trends for ERA5 time series over 2004-2021. Panels (b) and (c) show the longitudinally resolved trends at 32 km for ERA5 and TOMCAT, respectively.
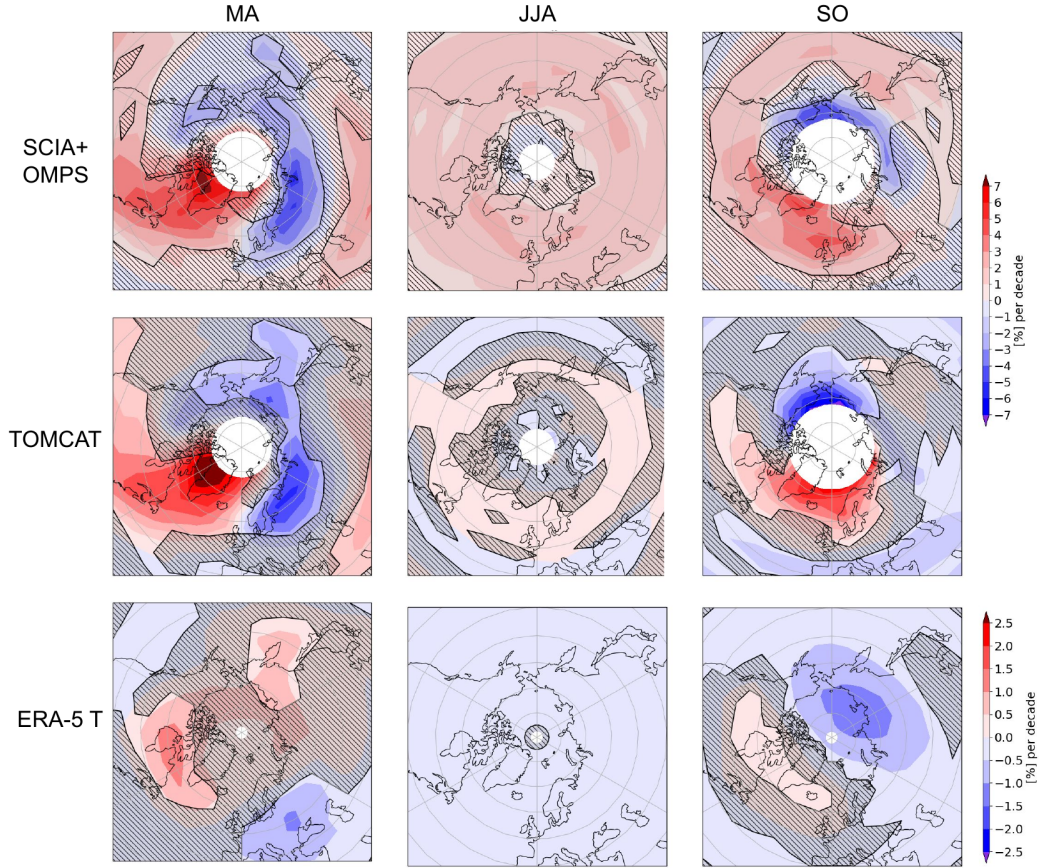
Figure 7. Seasonally resolved trends at 32 km from SCIA+OMPS dataset (top row), TOM-CAT reference simulation (middle row) and ERA5 temperature (bottom row). The left column shows trends for spring (MA), the middle column for summer (JJA) and the right one for autumn (SO).

During summer (JJA, middle column) the trend fields are fairly homogeneous over longitude, displaying significant positive values of about 1 % per decade for SCIA+OMPS and close to zero for TOMCAT. In contrast, during spring (left column) and autumn (right column) the asymmetry is well pronounced. In particular, we notice a strong zonal asymmetry in the spring-time trends in SCIA+OMPS that is very well captured by TOM-CAT, with the positive maximum located over the North Atlantic sector. The negative values between Scandinavia and Siberia are also statistically significant (at 2σ level) for both observations and model. A similar bi-polar pattern is also found in SO, but more confined to polar latitudes and shifted in longitude. The good agreement of TOMCAT with observations also holds in this case.

Regarding temperature, in summer we find a close-to-zero negative trend, whereas in spring and autumn the pattern is also zonally asymmetric, however no strong correlation with the patterns observed in the ozone trends was found. In conclusion, we find no strong evidence to relate the catalytic destruction of ozone in the polar vortex to the longitudinal asymmetry pattern observed in the Arctic.

A comparison between TOMCAT and SCIA+OMPS during winter months is more difficult, as limb scattering observations do not sample polar night conditions, as shown

in Fig. 8, panel (a), where trends in DJF are shown at 32 km. SCIA+OMPS shows large positive values with maxima over Canada and Scandinavia. The CTM, sampled in the same manner as the SCIA+OMPS monthly time series, shows a comparable pattern (panel (b)), with less pronounced positive values. The trends calculated using the full TOM-CAT profiles (non-sampled, averaged over all the model time steps) give a better picture of the two positive (over Canada and Scandinavia) and two negative cores (over Siberia and South of Greenland), although mostly not statistically significant.
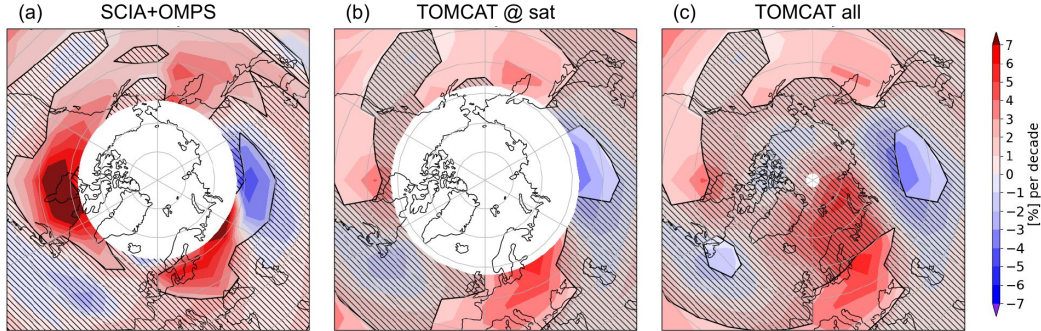
Figure 8. Seasonally resolved trends in winter at 32 km from SCIA+OMPS (panel a) and TOMCAT: in panel (b) the CTM simulation was sampled as the satellite data whereas in panel (c) the non-sampled TOMCAT times series was used to compute the trends.

6 Changes in GPH and atmospheric dynamics

To investigate changes in the wave activity at northern high latitudes during the last two decades as a cause of the asymmetry in trends, we analyzed the time series of geopotential height (GPH) from ERA5. In particular, we considered the longitudinally resolved vertical structure of the GPH field and decomposed it in wavenumber one (wave-1) and wavenumber two (wave-2) components, using a fast Fourier transform. We focused on the January-March period, where the largest asymmetric pattern in trends was found. This analysis is based on the theory of linear interference of waves (Smith & Kushner, 2012), according to which a negative correlation exists between changes in the climatological stationary wavefield and the stratospheric jet strength.

First we obtained the 2004-2021 climatology of the wave-1 component, after averaging the GPH over the [45° N, 70° N] latitude band. Then, we computed the linear trends of the wave-1 component over the same time period. Fig. 9a shows the wave-1 climatology in colors and the respective linear trends in m per decade in contours. The position of the positive wave-1 GPH anomalies is approximately collocated with the region showing a negative trend, and vice-versa, i.e. they are approximately in quadrature. In particular, a 100/120° eastward shift between the climatology and the wave-1 trend maxima is visible, pointing out an eastward shift in the wave-1 forcing and a weakening of the wavenumber-1 planetary wave, according to the linear wave theory (Matsuno, 1970), over the last two decades.

We then performed a similar analysis for the ozone field, choosing the TOMCAT time series with a complete coverage of the polar regions. We find a similar baroclinic pattern in the climatology of the wave-1 component of TOMCAT ozone particularly in the middle stratosphere, as shown in Fig. 9, panel (b). Above 5.0 hPa and below 50.0 hPa the correlation between the two panels breaks down. The trends of the ozone anomaly wave-1 component are superimposed in panel (b) in ppmv per decade and they are, sim-
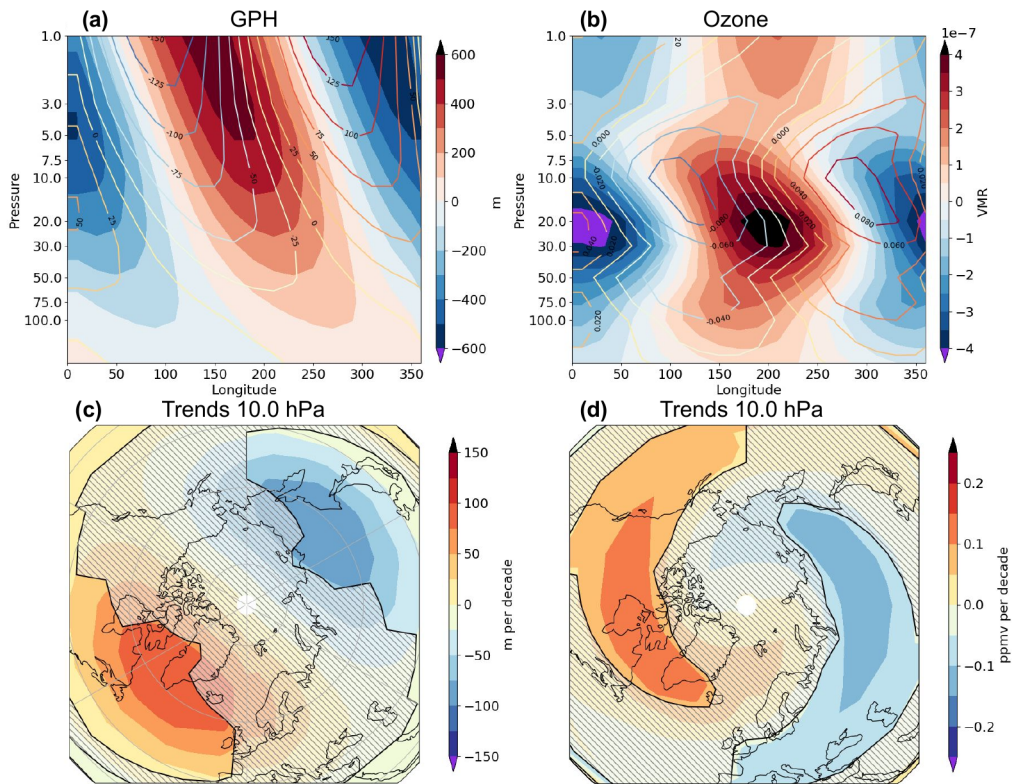
Figure 9. Top row, JFM climatology of the wave-1 component of GPH (left) and TOMCAT ozone (right) averaged over [45° N, 70° N]. Superimposed the trends of the same quantities are shown as contours, with values in m per decade (left) and ppmv per decade (right). Bottom row, the wave-1 trend values at 10.0 hPa are shown (striped regions indicate no statistical significance at 2σ).

ilarly to GPH, out of phase w.r.t. their climatological values. Panels (c) and (d) show the GPH and ozone trends at 10.0 hPa, respectively, with the striped areas indicating values smaller than their 1σ uncertainty. The similarity is evident, although the shape of the two cores is more elongated for ozone trends.
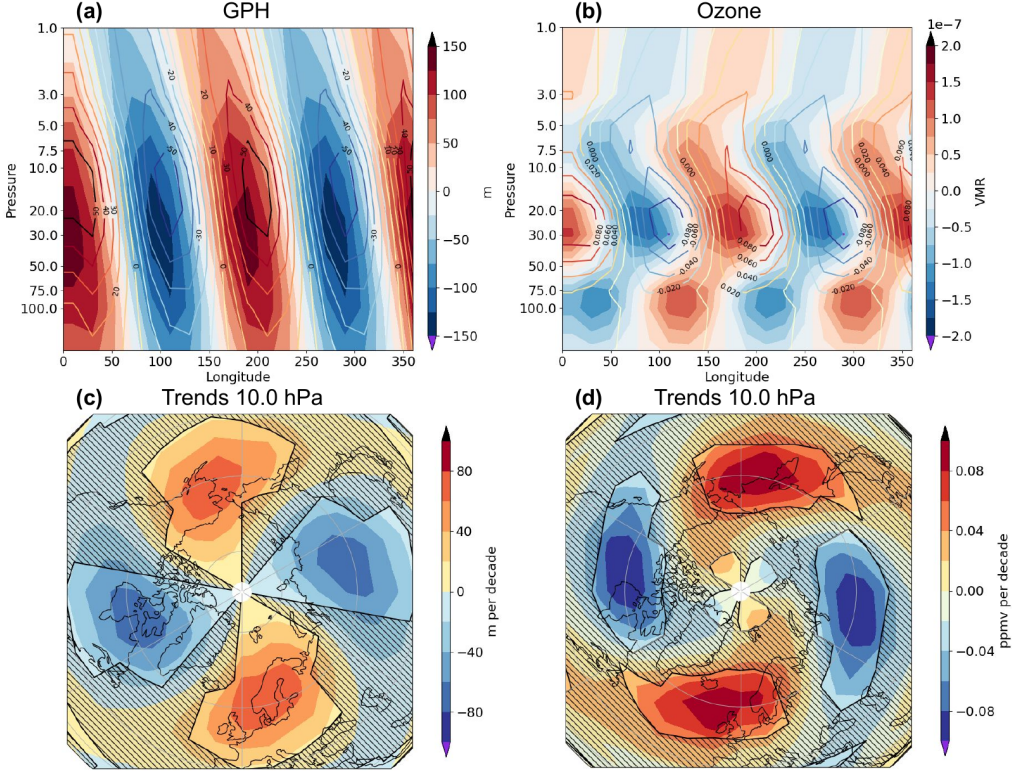
Figure 10. Same as Fig. 9, but for the wave-2 components of GPH and ozone.

As shown in Fig. 10, a similar analysis was performed for the wave-2 components of ERA5 GPH and TOMCAT ozone anomalies. The climatologies of wave-2 GPH and ozone anomalies in the middle stratosphere show again a baroclinic structure, with values that are approximately in phase with their respective trends (about $30°$ east-shift between the two maxima or minima). This indicates that the wavenumber-2 wave forcing in the stratosphere has intensified in the last 2 decades. Panels (c) and (d) show the wave-2 GPH and ozone trends at 10.0 hPa, respectively. The similarity is in this case striking.

To quantify the correlation between climatology and trends, we calculated the pressure-weighted pattern correlation as in Fletcher and Kushner (2011) for the GPH pattern and found a correlation of -0.75 for wave-1, i.e. out of phase, and of 0.77 for wave-2, i.e. close to in-phase. This analysis of the wave-1 and -2 components points out the strong correlation between changes in ozone and in GPH, which are themselves related to changes in wave activity. In our case, the pattern in GPH wave-1 and -2 components is consistent with a long-term shift and a strengthening of the polar vortex: the weakining and shift of the wavenumber-1 planetary wave activity is leading to a strengthening of the polar vortex, partially offset by the strengthening of the wavenumber-2 wave activity. This seems to be the main driver of the asymmetry in the long-term ozone changes.

The identified GPH patterns are consistent with previous literature findings, e.g., Hu et al. (2018), which were related by the authors to a weakening of the Aleutian low and to warmer sea-surface temperature over the central North Pacific. However other authors, e.g., Zhang et al. (2016); Seviour (2017), pointed out a weakening of the polar vortex over the 1980-2010 period. In the next Sect. we directly investigate changes in the polar vortex over the last 4 decades to reconcile these findings.

7 Potential vorticity trends and polar vortex changes

In this section we present the changes in the polar vortex over the last four decades, following studies such as Zhang et al. (2016). We defined the polar vortex boundary using the methodology described in Nash et al. (1996); in particular, we used ERA5 modified potential vorticity at 700 K and wind on potential vorticity isolines. 700 K is considered to be representative of the middle stratosphere, around 30 km. The determination of the polar vortex boundary is based on the peak of the potential vorticity gradient in the equivalent latitude space (Butchart & Remsberg, 1986), collocated with a horizontal wind peak. After determining the polar vortex boundary for the Februaries since 1980, we investigated the change in its position and strength.

We defined two relevant sectors where the ozone asymmetric pattern is relevant: the first around Greenland and the second over Siberia, as shown in the Supplements in Fig. S3. We computed the polar vortex relative occupancy of these two sectors in each February to assess decadal oscillations in the position of the polar vortex. As shown in Fig. 11, a change in the linear trends of the sector occupancy occurred at the beginning of the century: as reported in Zhang et al. (2016) over the period 1980-2009 the polar vortex underwent a shift to the Eurasian sector, however, from the beginning of the century, an opposite shift seems to have occurred. This tendency is not, however, as sound as the shift in the previous period, as several years (1987, 2006, 2009, 2013 and 2019) needs to be screened out, because of a weak polar vortex or major sudden stratospheric warming (SSW) events in February. Due to the high interannual variability, trends are mostly not significant, even at 1σ level as reported in the panels, and should be considered as decadal oscillations rather than a long-term change of the polar vortex.

In panel (c) of Fig. 11 the mean potential vorticity inside the polar vortex is shown: in the first two decades a negative linear trend is found, i.e. a weakening of the polar vortex as reported by Zhang et al. (2016) and Seviour (2017). In the last two decades, in contrast, the trend becomes positive, indicating a strengthening of the polar vortex as reported by Hu et al. (2018). The strengthening of the polar vortex is consistent with a positive shift in the Arctic oscillation (Weber et al., 2022).

Finally, we investigate the trends of the modified potential vorticity in the middle stratosphere (700 K) over the two periods 1980-2004 and 2000-2022. In Fig. 12 top panels, we clearly see a reversal of the pattern over the polar regions, with panel (a) showing similar results to the findings of Zhang et al. (2016), pointing out a shift of the polar vortex to Eurasia, whereas panel (b) indicates a shift of its mean position again towards North America over the last 20 years. Looking at the ozone trends on the 700 K isoentropic surface from the TOMCAT time series in the respective periods, shown in the bottom row of Fig. 12, we also notice a reversal of the pattern: the negative values were largest over the Atlantic/Scandinavian sector during the first period, whereas during the last two decades the positive trends are largest in the same region.
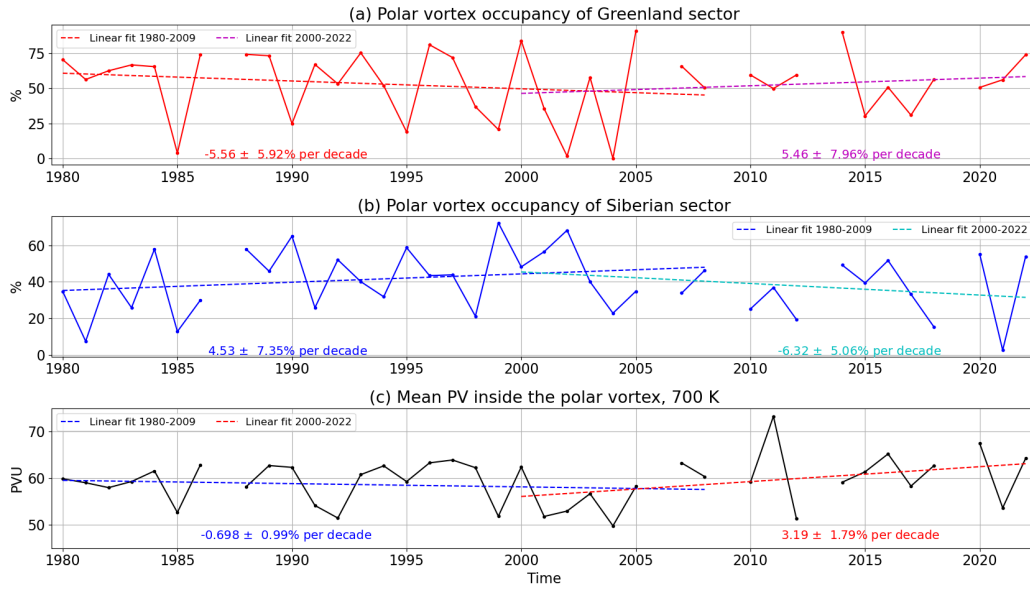
Figure 11. Panels (a) and (b) show the relative occupancy of the Greenland sector and of the Siberian sector, respectively, by the polar vortex. Panel (c) shows the mean modified potential vorticity within the polar vortex at 700 K isentropic surface. Respective trends with 1σ uncertainties are reported in the panels.
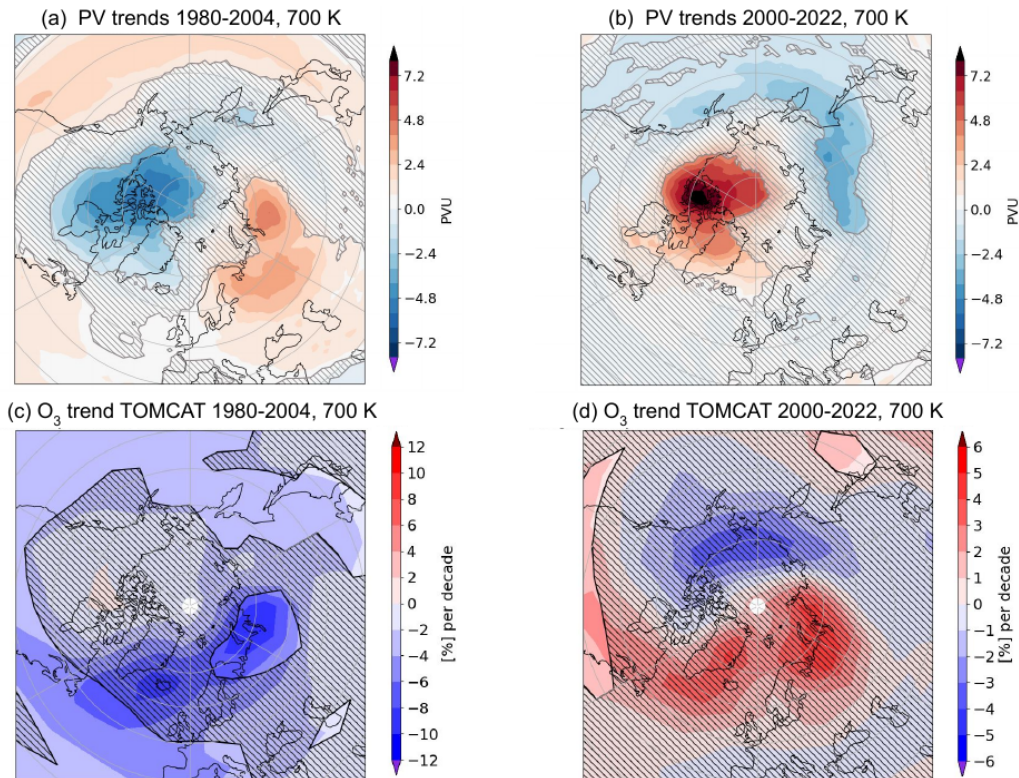

Figure 12. Trends of the ERA5 modified potential vorticity (panels (a) and (b)) and of the TOMCAT ozone (panels (c) and (d)) at the 700 K isentropic surface are shown for the periods 1980-2005 and 2000-2022.

8 Conclusions

In this study we have presented a comparison between satellite limb observations and simulations from the TOMCAT CTM to investigate the zonal asymmetry in ozone trends identified at northern high latitudes. The OMPS-LP product has been recently updated at the University of Bremen by using the improved L1G data provided by the NASA team, leading to a better long-term stability of the ozone time series w.r.t. the previous version. A preliminary comparison between SCIA+OMPS and TOMCAT time series and zonal trends demonstrated the overall good agreement between the two, when considering deseasonalized anomalies. We then presented the longitudinal asymmetry in trends observed at northern high latitudes over the period 2004-2021, which is well captured not only by the CTM but also by the ERA5 time series, hinting at the dynamical origin of this feature.

By using dedicated TOMCAT runs, we further showed that the identified patterns are dynamically driven, as neither gas-phase chemistry nor heterogeneous chemistry was found to have a relevant direct role in the discussed asymmetry. By investigating the trends at a seasonal level, we found that the asymmetry shows the largest amplitude in late winter/early spring. In this season, we found positive values up to 6-7 % per decade over Greenland and negative values of 3-4 % per decade over Eurasia. This seasonal trend pattern observed in SCIA+OMPS is very well reproduced by TOMCAT.

We decomposed ERA5 geopotential height (GPH) and TOMCAT ozone fields in wave-1 and -2 components for months JFM, finding a strong similarity in the changes of the two quantities in the middle stratosphere. According to the linear wave interference, the findings are consistent with a long-term shift and a strengthening of the polar vortex, i.e. weakening of the wavenumber-1 planetary wave. In this way, it was possible to link the zonal asymmetric pattern in ozone trends to changes in the wave activity in the stratosphere.

The analysis of the polar vortex position and of the trends in potential vorticity in the middle stratosphere in Sect. 7 qualitatively confirms the proposed relationships between the shift in the mean polar vortex position and the ozone trend asymmetry. The overall pattern underwent decadal changes over the last 40 years, with the last 2 decades seeing a probable strengthening of the vortex and a shift towards North America. This final section of the manuscript is related to the study of the long-term variations of the polar vortex due to climate change and requires further investigations to understand its causes.

In summary, this study has pointed out the role of decadal variations in atmospheric dynamics in explaining ozone trends at northern high latitudes. The observed asymmetry of ozone trends during the past decades is a consequence of decadal climate variability originating in the troposphere. This asymmetric pattern shall be taken into account when calculating ozone trends in the polar region in particular when using ground-based observations, e.g., ozonesondes and Fourier transform infrared spectrometers.

Appendix A Methods to merge SCIAMACHY and OMPS-LP datasets

For the study of seasonal trends, two approaches have been employed. In the first case, we compute the seasonal averages of the merged monthly SCIA+OMPS dataset. In the second case, the merging is applied to seasonal averages of both dataset anomalies. A filtering is necessary to remove latitude bins for which not all months in the defined season are available or when the latitude coverage of the two instruments differs (at high latitudes). It was found that the second method provides better agreement with CTM simulations compared to the first approach.

This is illustrated using, as an example, the March-April (MA) trends at 32 km displayed in Fig.A1. The "SCIA+OMPS post" indicates the computation of seasonal averages using the merged monthly dataset (first method), whereas the case "SCIA+OMPS pre" in the middle panel indicates the merging performed on seasonal averages (second method). The comparison with TOMCAT significantly improves in the second case.
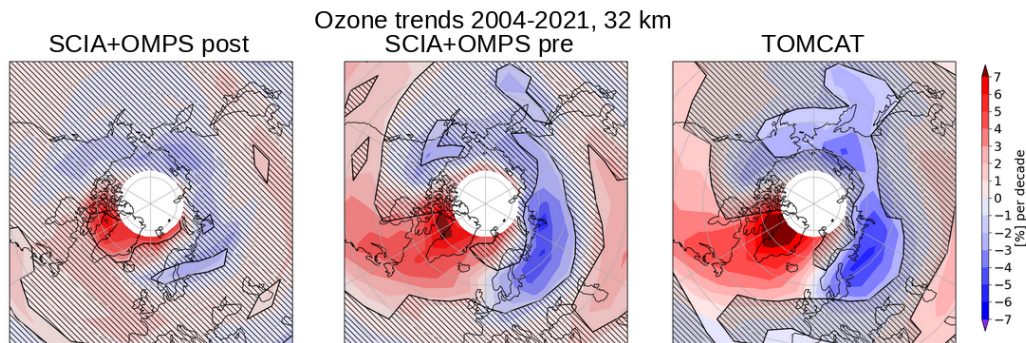

Figure A1. Comparison of seasonal ozone trends in MA at 32 km from SCIA+OMPS (leftmost two panels) and TOMCAT (right panel). In the left panel, the merging of the two satellite datasets is performed in terms of monthly time series ("post"); in the central panel, the merging is in terms of averaged seasonal values ("pre").

Open Research Section

The Merged SCIA+OMPS dataset produced at the University of Bremen and used for this study is available at the following link: https://doi.org/10.5281/zenodo.10033299. TOMCAT simulations and the extracted PV and GPH values used for this study can be found, respectively, at: https://zenodo.org/doi/10.5281/zenodo.10054832 and https://doi.org/10.5281/zenodo.10054575

References

Arosio, C., Rozanov, A., Malinina, E., Weber, M., & Burrows, J. P. (2019). Merging of ozone profiles from sciamachy, omps and sage ii observations to study stratospheric ozone changes. *Atmospheric Measurement Techniques*, *12*(4), 2423–2444.

Ball, W. T., Alsing, J., Mortlock, D. J., Staehelin, J., Haigh, J. D., Peter, T., . . . others (2018). Evidence for a continuous decline in lower stratospheric ozone offsetting ozone layer recovery. *Atmospheric Chemistry and Physics*, *18*(2), 1379–1394.

Bari, D., Gabriel, A., Körnich, H., & Peters, D. (2013). The effect of zonal asymmetries in the brewer-dobson circulation on ozone and water vapor distributions in the northern middle atmosphere. *Journal of Geophysical Research: Atmospheres*, *118*(9), 3447–3466.

Bernet, L., Boyd, I., Nedoluha, G., Querel, R., Swart, D., & Hocke, K. (2020). Validation and trend analysis of stratospheric ozone data from ground-based observations at lauder, new zealand. *Remote sensing*, *13*(1), 109.

Butchart, N. (2014). The brewer-dobson circulation. *Reviews of geophysics*, *52*(2), 157–184.

Butchart, N., & Remsberg, E. E. (1986). The area of the stratospheric polar vortex as a diagnostic for tracer transport on an isentropic surface. *Journal of Atmospheric Sciences*, *43*(13), 1319–1339.

Chipperfield, M. (2006). New version of the tomcat/slimcat off-line chemical transport model: Intercomparison of stratospheric tracer experiments. *Quarterly Journal of the Royal Meteorological Society: A journal of the atmospheric sciences, applied meteorology and physical oceanography*, *132*(617), 1179–1203.

Chipperfield, M. P., Dhomse, S., Hossaini, R., Feng, W., Santee, M. L., Weber, M., . . . Coldewey-Egbers, M. (2018). On the cause of recent variations in lower stratospheric ozone. *Geophysical Research Letters*, *45*(11), 5718-5726.

Dhomse, S. S., Arosio, C., Feng, W., Rozanov, A., Weber, M., & Chipperfield, M. P. (2021). Ml-tomcat: machine-learning-based satellite-corrected global stratospheric ozone profile data set from a chemical transport model. *Earth System Science Data*, *13*(12), 5711–5729.

Fletcher, C. G., & Kushner, P. J. (2011). The role of linear interference in the annular mode response to tropical sst forcing. *Journal of Climate*, *24*(3), 778–794.

Galytska, E., Rozanov, A., Chipperfield, M. P., Dhomse, S. S., Weber, M., Arosio, C., . . . Burrows, J. P. (2019). Dynamically controlled ozone decline in the tropical mid-stratosphere observed by sciamachy. *Atmospheric Chemistry and Physics*, *19*(2), 767–783.

Garcia, R. R., & Randel, W. J. (2008). Acceleration of the brewer–dobson circulation due to increases in greenhouse gases. *Journal of the Atmospheric Sciences*, *65*(8), 2731–2739.

Godin-Beekmann, S., Azouz, N., Sofieva, V. F., Hubert, D., Petropavlovskikh, I., Effertz, P., . . . others (2022). Updated trends of the stratospheric ozone vertical distribution in the 60° s–60° n latitude range based on the lotus regression model. *Atmospheric Chemistry and Physics*, *22*(17), 11657–11673.

Groves, K., Mattingly, S., & Tuck, A. (1978). Increased atmospheric carbon dioxide and stratospheric ozone. *Nature*, *273*(5665), 711–715.

Hood, L., & Zaff, D. A. (1995). Lower stratospheric stationary waves and the longitude dependence of ozone trends in winter. *Journal of Geophysical Research: Atmospheres*, *100*(D12), 25791–25800.

Hu, D., Guan, Z., Tian, W., & Ren, R. (2018). Recent strengthening of the stratospheric arctic vortex response to warming in the central north pacific. *Nature Communications*, *9*(1), 1697.

Hubert, D., Lambert, J.-C., Verhoelst, T., Granville, J., Keppens, A., Baray, J.-L., . . . others (2016). Ground-based assessment of the bias and long-term

stability of 14 limb and occultation ozone profile data records. *Atmospheric measurement techniques*, *9*(6), 2497–2534.

Karpechko, A. Y., Afargan-Gerstman, H., Butler, A. H., Domeisen, D. I., Kretschmer, M., Lawrence, Z., ... Wu, Z. (2022). Northern hemisphere stratosphere-troposphere circulation change in cmip6 models: 1. inter-model spread and scenario sensitivity. *Journal of Geophysical Research: Atmospheres*, *127*(18), e2022JD036992.

Kozubek, M., Krizan, P., & Lastovicka, J. (2015). Northern hemisphere stratospheric winds in higher midlatitudes: longitudinal distribution and long-term trends. *Atmospheric chemistry and physics*, *15*(4), 2203–2213.

Kozubek, M., Krizan, P., & Lastovicka, J. (2017). Comparison of the long-term trends in stratospheric dynamics of four reanalyses. In *Annales geophysicae* (Vol. 35, pp. 279–294).

Kramarova, N. A., Bhartia, P. K., Jaross, G., Moy, L., Xu, P., Chen, Z., ... others (2018). Validation of ozone profile retrievals derived from the omps lp version 2.5 algorithm against correlative satellite measurements. *Atmospheric Measurement Techniques*, *11*(5), 2837–2861.

Li, Y., Dhomse, S. S., Chipperfield, M. P., Feng, W., Bian, J., Xia, Y., & Guo, D. (2023). Stratospheric ozone trends and attribution over 1984–2020 using ordinary and regularised multivariate regression models. *EGUsphere*, *2023*, 1–24.

Li, Y., Dhomse, S. S., Chipperfield, M. P., Feng, W., Chrysanthou, A., Xia, Y., & Guo, D. (2022). Effects of reanalysis forcing fields on ozone trends and age of air from a chemical transport model. *Atmospheric Chemistry and Physics*, *22*(16), 10635–10656.

Lu, J., Lou, S., Huang, X., Xue, L., Ding, K., Liu, T., ... Ding, A. (2023). Stratospheric aerosol and ozone responses to the hunga tonga-hunga ha'apai volcanic eruption. *Geophysical Research Letters*, *50*(4), e2022GL102315.

Matsuno, T. (1970). Vertical propagation of stationary planetary waves in the winter northern hemisphere. *Journal of Atmospheric Sciences*, *27*(6), 871–883.

McIntyre, M., & Palmer, T. (1984). The 'surf zone'in the stratosphere. *Journal of atmospheric and terrestrial physics*, *46*(9), 825–849.

Nash, E. R., Newman, P. A., Rosenfield, J. E., & Schoeberl, M. R. (1996). An objective determination of the polar vortex using ertel's potential vorticity. *Journal of Geophysical Research: Atmospheres*, *101*(D5), 9471–9478.

Peters, D., & Entzian, G. (1999). Longitude-dependent decadal changes of total ozone in boreal winter months during 1979–92. *Journal of climate*, *12*(4), 1038–1048.

Petropavlovskikh, I., Godin-Beekmann, S., Hubert, D., Damadeo, R., Hassler, B., & Sofieva, V. (2019). *Sparc/io3c/gaw report on long-term ozone trends and uncertainties in the stratosphere* (Vols. SPARC Report No. 9, WCRP-17/2018, GAW Report No. 241). doi: https://doi.org/10.17874/f899e57a20b

Seinfeld, J. H., & Pandis, S. N. (2016). *Atmospheric chemistry and physics: from air pollution to climate change.* John Wiley & Sons.

Seviour, W. J. (2017). Weakening and shift of the arctic stratospheric polar vortex: Internal variability or forced response? *Geophysical Research Letters*, *44*(7), 3365–3373.

Smith, K. L., & Kushner, P. J. (2012). Linear interference and the initiation of extratropical stratosphere-troposphere interactions. *Journal of Geophysical Research: Atmospheres*, *117*(D13).

Sofieva, V. F., Kyrölä, E., Laine, M., Tamminen, J., Degenstein, D., Bourassa, A., ... others (2017). Merged sage ii, ozone_cci and omps ozone profile dataset and evaluation of ozone trends in the stratosphere. *Atmospheric Chemistry and Physics*, *17*(20), 12533–12552.

Sofieva, V. F., Szelag, M., Tamminen, J., Kyrölä, E., Degenstein, D., Roth, C., ...

others (2021). Measurement report: regional trends of stratospheric ozone evaluated using the merged gridded dataset of ozone profiles (megridop). *Atmospheric Chemistry and Physics*, *21*(9), 6707–6720.

Waugh, D., Oman, L., Kawa, S., Stolarski, R., Pawson, S., Douglass, A., ... Nielsen, J. (2009). Impacts of climate change on stratospheric ozone recovery. *Geophysical Research Letters*, *36*(3).

Weber, M., Arosio, C., Coldewey-Egbers, M., Fioletov, V. E., Frith, S. M., Wild, J. D., ... Loyola, D. (2022). Global total ozone recovery trends attributed to ozone-depleting substance (ods) changes derived from five merged ozone datasets. *Atmospheric Chemistry and Physics*, *22*(10), 6843–6859.

WMO. (2018). *Scientific Assessment of Ozone Depletion 2018, Global Ozone Research and Monitoring Project Report 58.* World Meterological Organization. Retrieved from `https://csl.noaa.gov/assessments/ozone/2018/downloads/2018OzoneAssessment.pdf`

WMO. (2022). *Scientific Assessment of Ozone Depletion 2022, Global Ozone Research and Monitoring Project Report 59.* World Meterological Organization. Retrieved from `https://csl.noaa.gov/assessments/ozone/2022/downloads/2022OzoneAssessment.pdf`

Zhang, J., Tian, W., Chipperfield, M. P., Xie, F., & Huang, J. (2016). Persistent shift of the arctic polar vortex towards the eurasian continent in recent decades. *Nature Climate Change*, *6*(12), 1094–1099.